ELSEVIER

Contents lists available at ScienceDirect

Earth and Planetary Science Letters

www.elsevier.com/locate/epsl



Complex upper mantle anisotropy in the Pacific Northwest: Evidence from SKS splitting



William Niday*, Eugene Humphreys

Department of Earth Sciences, University of Oregon, Eugene, OR 97403-1272, USA

ARTICLE INFO

Article history: Received 17 November 2019 Received in revised form 28 March 2020 Accepted 4 April 2020 Available online 20 April 2020 Editor: M. Ishii

Keywords: seismic anisotropy shear wave splitting Pacific Northwest asthenosphere

ABSTRACT

We use a dense network of observations and an automated method of analysis to investigate complex patterns of seismic anisotropy in the Pacific Northwest. We present SKS splitting results for approximately 220 broadband seismic stations, including 33 stations from the new Wallowa2 array deployed between 2016 and 2018 in northeast Oregon. Our data set contains approximately 3300 splitting measurements. Our anisotropy measurements indicate that anisotropy in the Pacific Northwest can be divided into two domains: near the subduction zone, anisotropy is perpendicular to the slab; and inboard of the subduction zone anisotropy tends to parallel the velocity structure and is roughly oriented with "absolute" plate motion. However, splitting analysis performs poorly in northeast Oregon, and results are not consistent with uniform or layered anisotropy. We argue that the complex splitting behavior in northern Oregon is a result of spatially variable upper mantle anisotropy, related to the complex upper mantle seismic structure. Interpreting the mantle anisotropy in this region requires methods not limited to standard ray theoretical shear wave splitting analysis.

© 2020 Elsevier B.V. All rights reserved.

1. Introduction

Because shear deformation in the upper mantle produces a lattice preferred orientation (LPO) of anisotropic mineral crystals (mostly olivine), observations of seismic anisotropy can provide a valuable constraint on the geometry of mantle flow (Karato et al., 2008). Measuring the splitting of core-refracted shear waves such as SKS is one of the most well-studied and direct ways of quantifying seismic anisotropy. Because of its near vertical incidence, SKS splitting provides good constraints on lateral variation of anisotropy but little direct information about vertical variation. Furthermore, standard methods for shear-wave splitting analysis are most reliable when measuring one anisotropic system, which lies in the horizontal plane. If these assumptions do not hold, such as if the upper mantle is strongly heterogeneous on the scale of seismic wavelengths, the relationship between shear-wave splitting and anisotropy may be complex (e.g., Long and Silver, 2009).

Although no studies have focused on complex anisotropy in northeast Oregon, there are several avenues of evidence that bear on the region. Long et al. (2009) studied shear-wave splitting in eastern Oregon with the High Lava Plains and Wallowa1 broadband seismic networks, finding a relatively coherent east-west fast axis orientation with very large split times in southeast Oregon. For stations in northeast Oregon, they found fewer and less consistent splitting measurements, which they attributed to a component of lithospheric anisotropy (as opposed to pure asthenospheric flow in southeast Oregon).

Lin et al. (2011) fit observed shear-wave splitting with a model including surface wave measurements of crustal and uppermost mantle anisotropy and a smoothly varying asthenosphere, which performs well in most of the western U.S. but poorly in northeast Oregon (although few measurements were available). We also note that in the shear-wave splitting database of Yang et al. (2016), there are relatively few non-null measurements for stations in northeast Oregon despite a good station and back azimuth distribution. However, the splitting times for non-null measurements in northeast Oregon are significant (\sim 1.2 s), implying that the frequent null measurements are not simply a result of small or vertically oriented anisotropy.

In this study, we integrate data from the EarthScope USArray and several regional seismic arrays to investigate shear-wave splitting in the Pacific Northwest, with a focus on northeast Oregon. We use a very dense Wallowa1 and Wallowa2 networks of

^{*} Corresponding author.

E-mail addresses: wniday@uoregon.edu (W. Niday), genehumphreys@gmail.com
E. Humphreys).

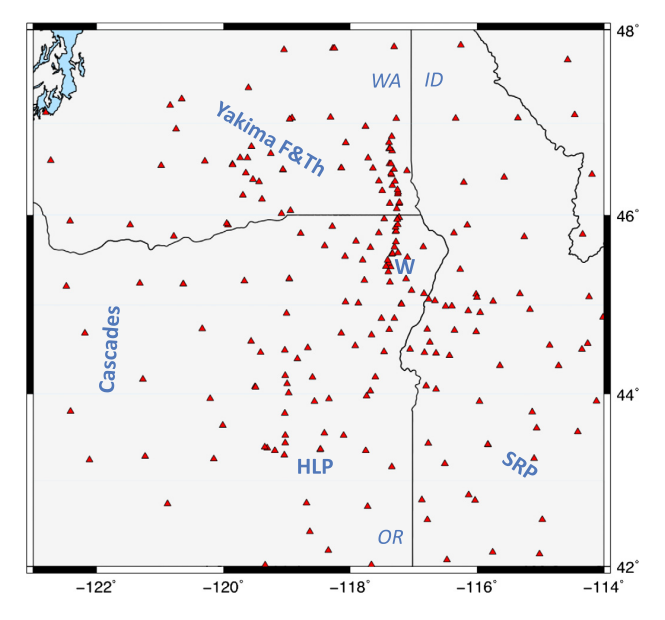


Fig. 1. Location of the broadband seismic stations used in this study. Study area shown on Fig. 2. Physiographic features: HLP = Lava Plains, SRP = Snake River Plain, W = Wallowa Mountains, Yakima F&Th = Yakima fold and thrust zone. States: ID = Idaho, OR = Oregon, WA = Washington.

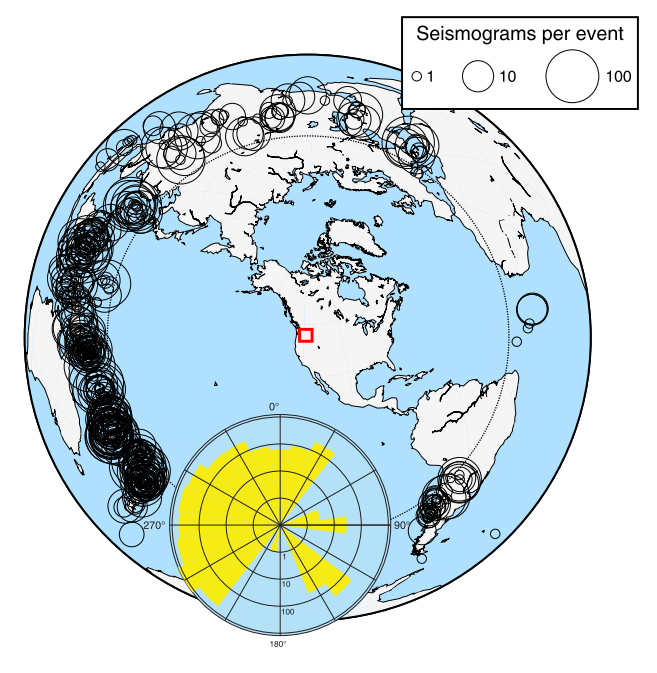


Fig. 2. Distribution of earthquake used in this study. The number of seismograms per earthquake indicated by symbol size. Red square shows our study area. Inset shows backazimuth distribution for all seismograms (note logarithmic scale). The dotted black line corresponds to a distance of 85°, and the border of the map corresponds to 120°.

broadband seismic observations to characterize splitting in the tectonically complicated region of northeast Oregon, and relate the anisotropy there to tomographically imaged upper mantle structures.

2. Methods

2.1. Data collection

We use data from approximately 220 broadband seismic stations in the IRIS DMC (Fig. 1). These include stations from the U.S. National Seismic Network, USArray Transportable Array, Pacific Northwest Seismic Network, and several campaign seismic arrays including recently acquired data from the IDOR and Wallowa2 arrays. We obtain seismograms for earthquakes magnitude (m_b and m_w) greater than 5.5 (usually greater than 6) and in the distance range of 85-120°, where the SKS phase amplitudes are significant. The resulting set of earthquakes is dominated by events with back azimuths between 225° and 315° (Fig. 2).

Radial SKS arrivals are automatically picked using a 30 second window centered around the estimated travel time from the TauP package (Crotwell et al., 1999). An automatic quality control step discards seismograms with a signal-to-noise ratio of less than three when band-pass filtered to between 0.02 and 0.25 Hz. The automatic picks are then manually checked to remove duplicate events and instrument errors, and ensure that the SKS window does not overlap with other phases. Approximately 5000 seismograms remain after quality control.

2.2. Splitting measurement

The most widely used methods for measuring shear-wave splitting from an individual record are the rotation correlation method [RC] (Bowman and Ando, 1987) and transverse component minimization method [SC] (Silver and Chan, 1991), both of which are implemented in the commonly used SplitLab package (Wüstefeld et al., 2008). Both methods assume that anisotropy produces two identically shaped, orthogonally polarized pulses, implying a vertically incident ray and a single horizontal anisotropic layer. More complex anisotropy results in frequent 'null splits' and azimuthal variation in 'apparent' splitting parameters. Variations in apparent splitting at a single station can be used to identify multilayered or dipping anisotropy (e.g., Silver and Savage, 1994), but this requires better azimuthal coverage than is typically available.

This study uses the cross-convolution method [ML] of Menke and Levin (2003) to measure shear-wave splitting. ML assumes that the observed radial (V(t)) and transverse (H(t)) waveforms are each the convolution of a common source wavelet s(t) with the impulse response functions $v_{true}(t)$ and $h_{true}(t)$. If an anisotropic model m has impulse responses v(m,t) and h(m,t), the model predicts radial and transverse waveforms $V_{pre}(t) = s(t) * v(m, t)$ and $H_{pre}(t) = s(t) * h(m, t)$. If m is a good model, then $V_{pre}(t) \approx$ V(t) and $H_{pre}(t) \approx H(t)$, and thus $v(m,t) * H(t) \approx h(m,t) * V(t)$. We search for a model that minimizes the normalized difference E(m) between the two 'cross convolution' waveforms v(m,t) * H(t) and h(m, t) * V(t). Fig. 3 shows two examples of the crossconvolution method using synthetic data. The one-layer inversion of a one-layer input works nearly perfectly. With the one-layer inversion of a two-layer input significant unmodeled energy remains, indicating that anisotropy is more complex than the onelayer model; however, in the presence of modest noise it could be difficult to identify the second layer.

Since ML does not assume the fast and slow pulses are identically shaped, it can directly assess complex models without the need for apparent splitting parameters, and it does not require as complete a back-azimuth distribution (Menke and Levin, 2003). We also find it to be robust in the presence of pre-signal noise: compared to RC or SC, ML does not require manual input to select a filter (splitting analysis on the raw data produces consistent results) or choose a narrow time window around the SKS arrival.

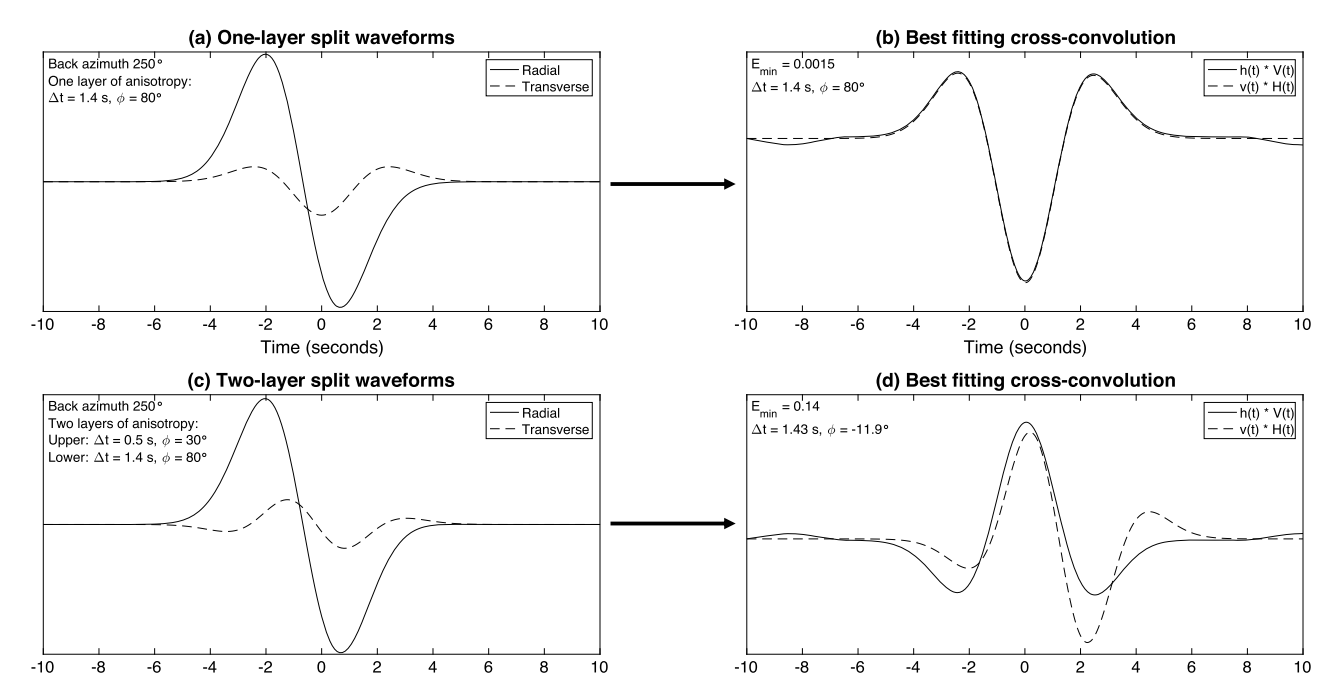


Fig. 3. Synthetic examples of the cross-convolution method. (a) Predicted radial and transverse waveforms due to one-layer anisotropy model. (b) Cross-convolution waveforms, predicted splitting parameters Δt and ϕ and misfit statistic E, modeled with a one-layer model applied to the waveforms in (a). V(t) is the observed radial waveform and v(t) is the model's radial component impulse response; similar for the transverse components H(t) and h(t). (c) Predicted radial and transverse waveforms due to two-layer anisotropy model. (d) Cross-convolution waveforms, predicted splitting parameters and misfit statistic, modeled with a one-layer model applied to the waveforms in (c).

Like the SC and RC methods, when a seismogram is noisy the ML method returns 'null-split' measurements, or the polarization direction coincides with the fast or slow direction of anisotropy, or the single-layer model does not fit the observations well. In the ML results, null measurements tend to have large split times and best-fitting models with fast directions parallel to the back azimuth. Null and noisy measurements do not need to be removed when calculating splitting parameters at a station, but we apply an additional automatic quality control step to remove these questionable results from our plots of results for individual events. We discard events with unreasonably large split times (>4 s), then discard events more than 2.5 standard deviations from the average of all events with piercing points within 50 km, where averaging is over the sine and cosine 2 theta coefficients. With nulls removed, the data set includes approximately 3100 measurements.

3. Results

Comparing seismograms across the region, we find that radial component SKS arrivals for the same events look similar at stations in NE and SE Oregon (Fig. 4). Transverse SKS arrivals often differ between stations (as expected, if anisotropy varies across the region), but we find that most events produce well defined transverse SKS arrivals across the region. We do not see a systematic difference in noise characteristics between stations in NE and SE Oregon.

The amplitude of the transverse component SKS signal (which is zero in the isotropic case) is consistently lower in NE Oregon than elsewhere. Long et al. (2009) found many null results (with no significant transverse component signal) at stations in NE Oregon, from a wide range of azimuths. We observe numerous events that produce no distinct transverse component signal at any of the stations in our study area, typically from back azimuths that coincide with the fast or slow axis of SKS splitting. We also find some events with a transverse signal that is observed across most

of our study area, but vanishes in NE Oregon. However, we also note several events with significant transverse component signals and corresponding large split times in NE Oregon. These events yield large split times at multiple NE Oregon stations, and they yield consistent anisotropy results for different back azimuths and incidence angles. We take these results to indicate the anisotropy beneath the NE Oregon stations, in spite of the occurrence of an overall complex splitting behavior.

To understand the effects of noise on our results, we corrected waveforms for the best-fitting set of single layer splitting parameters. In the case that the true anisotropy is a single layer, and in the absence of scattering of dipping anisotropy, this correction should remove all energy on the transverse seismogram (e.g., Silver and Chan, 1991). For our data, the presence of events that are well resolved as null from both NE and SE Oregon (which have back azimuths approximately coinciding with the fast axis in SE Oregon) lead us to infer an absence of significant, widespread scattering or dipping anisotropy. We observe a significant amount of transverse energy from NE Oregon events after correction (Fig. 4). The amplitude of the initial transverse component is smallest in NE Oregon, but the residual transverse component after correcting for one-layer splitting is largest in NE Oregon. Although there is no straightforward relationship between this residual signal and the anisotropy, the correspondence between the smallest transverse component amplitudes before the correction and the largest amplitudes after the correction implies that the anisotropic structure is more complex than a single-layer model.

3.1. Splitting results

We use the ML method to measure splitting for each seismogram assuming a single-layer model. The fast axes of shear wave splitting measured at stations (Fig. 5a) tend to be oriented east-northeast. Fast axes beneath the Blue Mountains trend more northeasterly, and trend to the southeast in the western Snake River

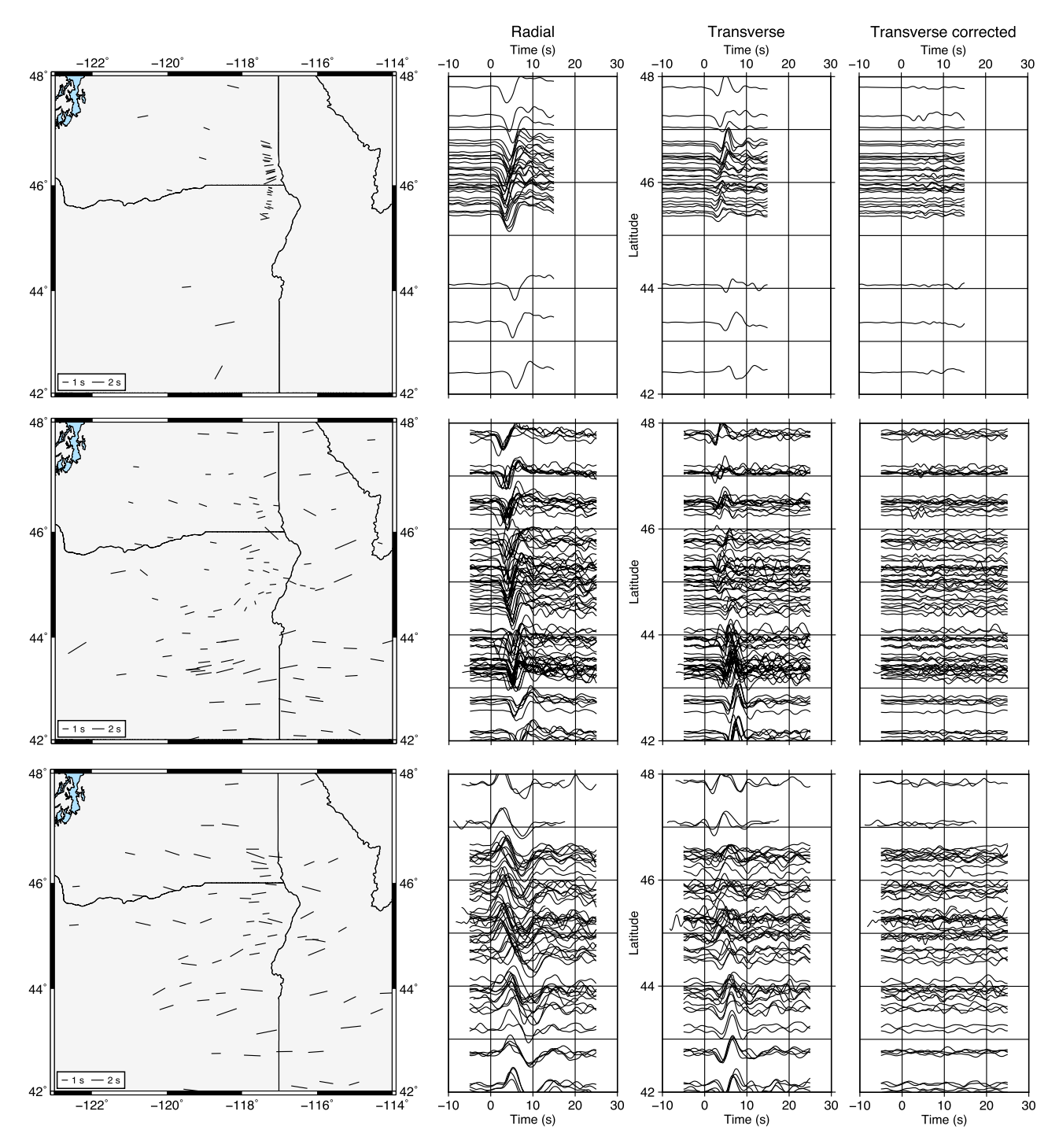


Fig. 4. Splitting results and waveforms for (top) low, (middle) moderate and (bottom) high-noise events. Transverse corrected' is the transverse component after applying the inverse operator for the best fitting one-layer splitting result on each waveform. Times on *x*-axis are offsets from the predicted SKS arrival time. Notice that especially in NE Oregon, significant energy remains on corrected transverse traces which far exceeds the pre-SKS noise level.

Plain. Split times are quite variable, with maximum split times of $\sim 2~\text{s}$ in the High Lava Plains and decreasing to an average of $\sim 1~\text{s}$ in northeast Oregon and nearby areas. Splitting measurements vary smoothly below stations, and we see no outliers among stations with > 10~measurements.

In Fig. 5b we back project the individual splitting events to their ray piercing points at a depth of 200 km (a depth chosen visually

to maximize the coherency of the plot). Because of the nonuniform distribution of global seismicity, our data are dominated by events with back azimuths to the west, and a large number of piercing points cluster to the west of the north-south oriented Wallowa2 array. The greater scatter in splitting parameters around NE Oregon is likely due in part to the large number of measurements in this area, but throughout the northern half of the study area

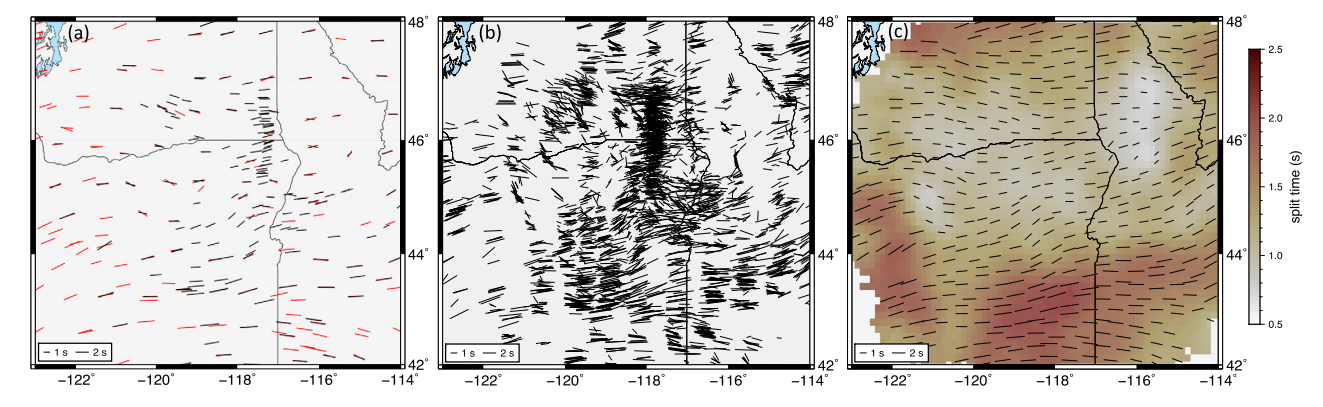


Fig. 5. SKS splitting results. (a) Station-average splitting estimates for stations with ≥ 10 events recorded (black), and results of Yang et al. (2016) (red). Line orientation shows the fast-axis polarization direction. (b) Individual non-null splitting results, plotted at the piercing points of the rays at 200 km depth. Line orientation shows the fast-axis polarization direction. (c) Splitting estimates, produced by stacking individual measurements at their 200 km piercing points in overlapping circular bins with radius of 50 km. The similarity between this field and splitting results at the stations (a) suggests that anisotropy to extends to a depth of ~ 200 km.

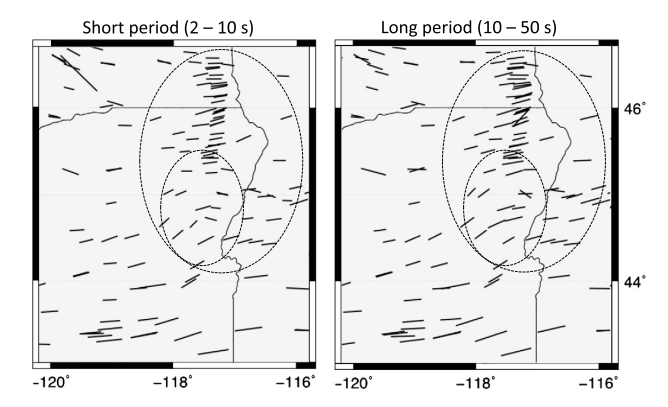


Fig. 6. Frequency dependence of anisotropy results. The small oval shows the region where anisotropy orientation varies strongly in east central Oregon. Splitting parameters are more spatially variable at short period. The large oval indicates where long-period split times are larger.

we note events with similar piercing points and different splitting measurements.

If complex SKS waveforms in NE Oregon were a result of near-field effects such as topographic signal-generated noise or crustal anisotropy, we would expect to see systematic differences between events with nearby piercing points at 200 km, when measured at separate stations (i.e., with rays sampling the same mantle volume, but different regions of the crust). However, we do not see such a difference – results with nearby piercing points are consistent from station to station. Well constrained measurements with significantly different parameters overlap, but the variation in parameters does not appear to depend on station location.

In Fig. 5c we resample the results from Fig. 5b onto a set of irregularly scattered points by summing the error surfaces of all events with piercing points within 50 km of the sample point. The results define an anisotropy field that varies smoothly in orientation and amplitude at a wavelength of \sim 150 km. In areas that are well covered by rays at 200 km depth, this map is similar to the station-averaged splitting map. We also tried two-layer models (discussed below), but with limited success. For events with published splitting measurements (e.g., Yang et al., 2016), ML results are typically very similar to other methods.

Splitting in both NE and SE Oregon varies somewhat depending on the frequency band, but for the most part the results are very similar. Fig. 6 shows splitting results east central Oregon, where a coherent lateral variation in anisotropy orientation is seen. We observe in the longer period (20-50 s) results both larger split times

(by 10-20%) and a smoother, less pronounced variation in orientation. This could suggest the local complexity is caused by relatively shallow structure (Saltzer et al., 2000), although the evidence is not compelling.

3.2. Complex anisotropy

As a simple way of assessing the evidence for complex anisotropy, we use the Menke and Levin (2003) misfit statistic E(m) of the individual measurements of this statistic at each station. A vertically incident ray on a uniform, flat anisotropic layer with a horizontal fast axis produces identically shaped fast and slow pulses, and in the absence of noise the two cross-convolution waveforms match perfectly (e.g., Fig. 3 a and b). If the anisotropy is more complex, the fast and slow pulses are not generally identically shaped, and the cross-convolution waveforms do not match (e.g., Fig. 3 c and d)

For both the stacked station model (Fig. 7a) and single event results (Fig. 7b), we observe coherent patterns in the geographical distribution of misfit. Misfit is generally low in the northern and southern parts of the study region and increases toward NE Oregon. However, even though the average misfit increases in NE Oregon we observe many individual results with small misfit values. Although noisier records have greater misfit values, records at stations in NE Oregon are not significantly noisier than in the rest of the study area. In the waveforms of well-recorded events (such as in Fig. 4), the amplitude of pre-SKS noise for the same event is similar in NE and SE Oregon, though there is significant variation in noise between events.

Fig. 8 shows the results of two-layer modeling. Where two-layer models are successful, one of the layers is typically oriented close to the orientation of the best-fitting single layer model. Menke and Levin (2003) note that two-layer models are prone to over-fitting because the four-parameter model (the fast axis orientation and split time for each layer) is nonunique, and a two layer model with nearly parallel or perpendicular fast axis orientations is nearly equivalent to a single layer model. The ML method can theoretically identify two layers of anisotropy from a single record, but given that two-layer models are poorly constrained we stacked results from events with nearby piercing points by summing the error surfaces. For each location we compare the misfit E(m) of the best fitting one- and two-layer models using an f-test, and only show two-layer models where they improve the misfit at a 95% confidence level.

The two-layer models often give a statistically significant improvement in the cross-convolution misfit, but misfit values remain

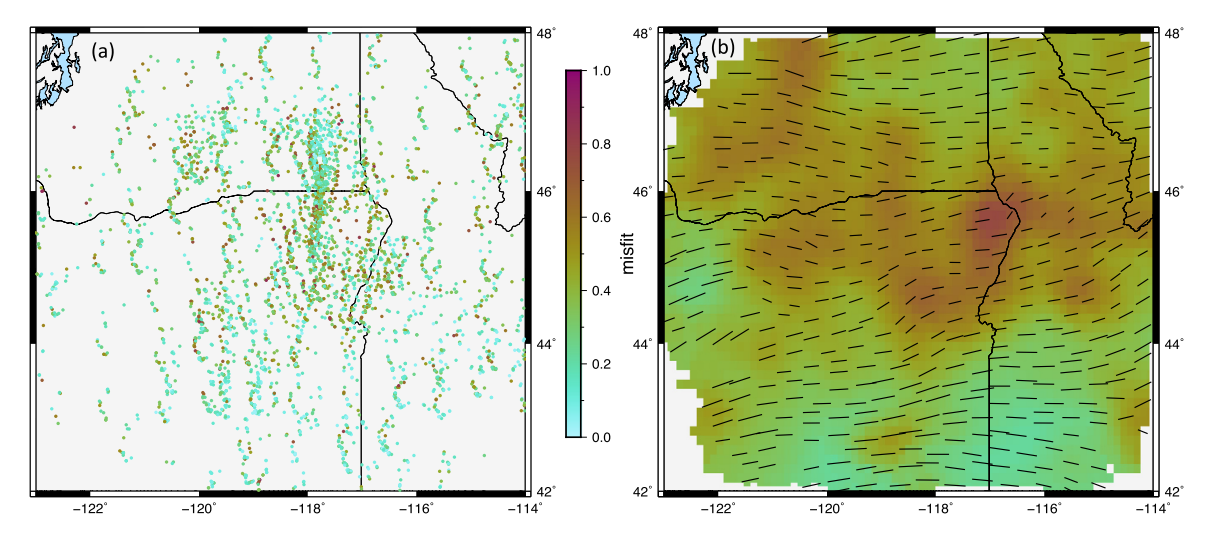


Fig. 7. Cross-convolution misfit, E(m). (a) Misfit of the best-fitting one-layer models for each event, plotted at the ray piercing points at 200 km depth. (b) Misfit of the stacked splitting estimates from Fig. 5c, stacked as described in that figure. Bars are the splitting results of Fig. 5c. The largest misfit values occur for events with northwest back azimuths, and overall misfit increases in northern Oregon.

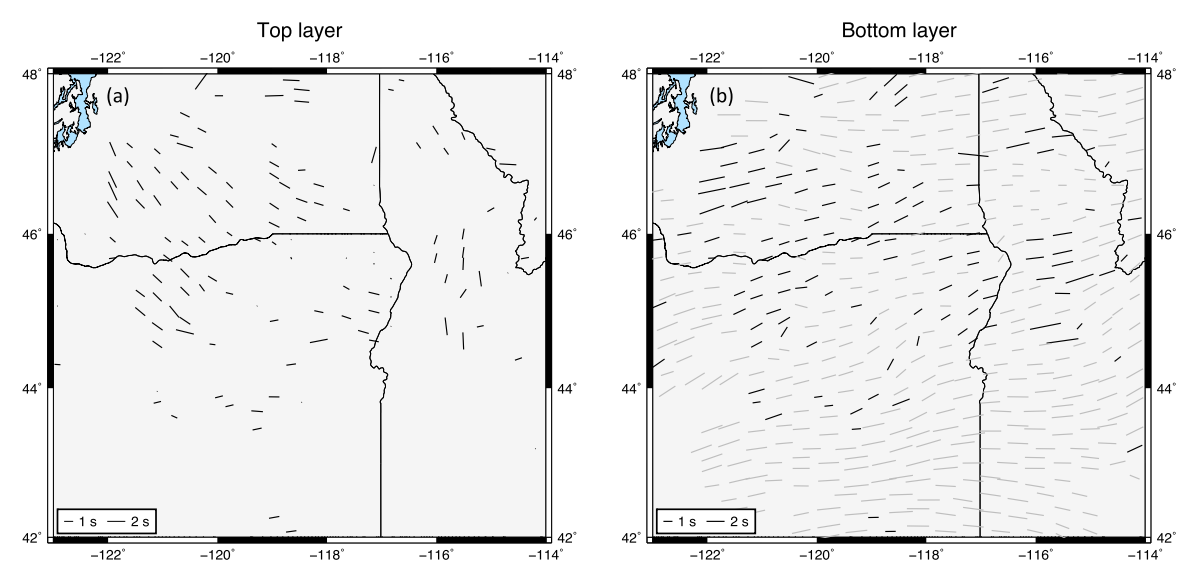


Fig. 8. Best fitting two-layer anisotropic models, produced by stacking individual measurements, as in Fig. 5c. Only two-layer models with a statistically significant (at the 95% level) improvement over the one-layer model are shown; if the improvement is not significant, we show the results of the one-layer model in the right frame. In the right frame, lighter gray markers indicate where the result shown is from the one-layer model. During modeling, when the layers have nearly perpendicular fast-axis orientations, the results of a two-layer model are very similar to those of a one-layer model. Results are generally coherent, and the bottom layer results are consistent with the single-layer model. However, regions where the two-layer model is successful do not correspond particularly well to regions where the one-layer misfit (Fig. 7b) is largest.

much larger in northeast Oregon. In many cases the best-fitting fast axes are near perpendicular and one layer is parallel to the single-layer model, suggesting that the variance reduction is due to overfitting of noise. The consistency of the results suggests that anisotropy varies with depth, but a two-layer model does not appear to describe anisotropy in northeast Oregon. However, we note that the most densely sampled area of the High Lava Plains produces successful two-layer models that do not fall in the "nearly one layer" regime, consistent with Wagner and Long's (2013) observations of strong vertical heterogeneity.

3.3. Finite frequency modeling

Given that the two-layer anisotropy model performs poorly in NE Oregon, we hypothesize that upper mantle anisotropy varies laterally. We use the three-dimensional finite-frequency sensitivity kernels of Favier and Chevrot (2003) to investigate the effects of spatially variable anisotropy on splitting. We calculate splitting intensity as a function of back azimuth using the sensitivity kernels, and predict station-averaged splitting by fitting a sine function as described by Chevrot (2000). Although the splitting as measured by splitting intensity is not necessarily the same as that measured by cross-convolution, we expect that results for the two methods are similar (Romanowicz and Yuan, 2012).

The Favier and Chevrot (2003) sensitivity kernels imply that a vertically incident shear wave at 0.1 Hz (typical for teleseismic SKS phases) at a depth of 200 km is sensitive to a mantle volume with a radius of approximately 150 km, and the peak sensitivity occurs approximately 60 km from the ray path. The observed split time is more sensitive to spatial variations in anisotropy than the ob-

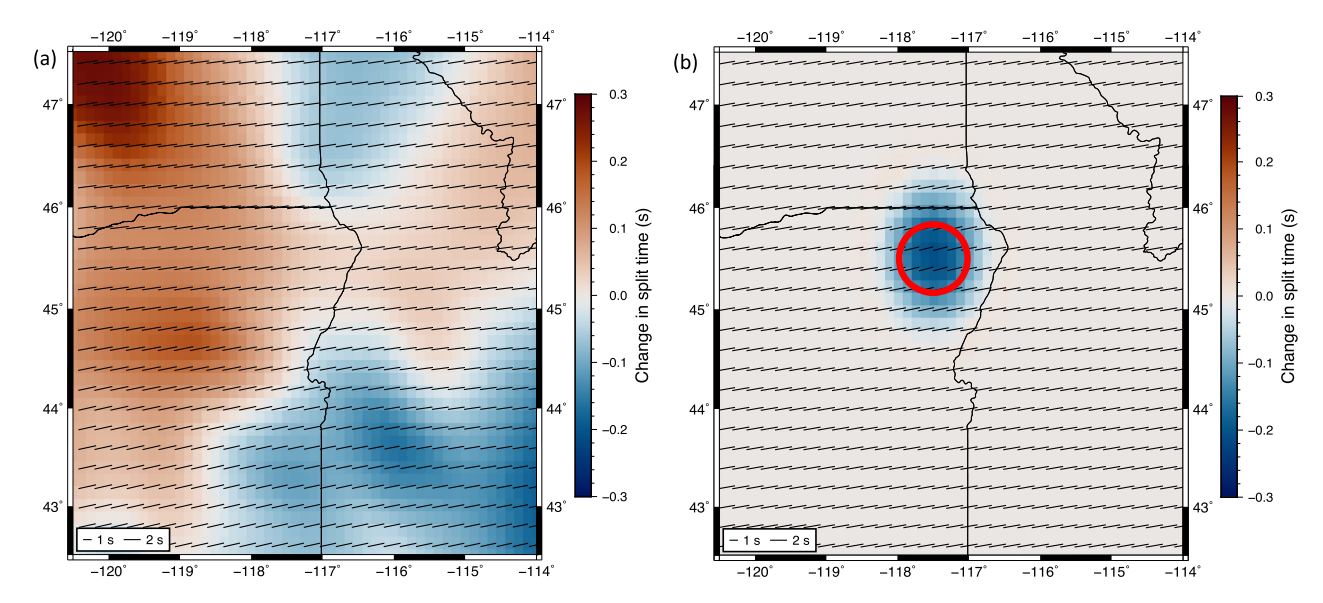


Fig. 9. (a) Illustration of the effect of an anisotropic upper mantle anomaly on SKS splitting. The model consists of the same 'mantle' layer as in (a), with a cylindrical upper mantle anomaly (indicated by the red circle) extending from a depth of 50-150 km with 3% anisotropy oriented N10° E. Observed fast directions are again unaffected, but the upper mantle anomaly causes a decrease in split times, which extends outside the anomaly itself because of finite-frequency effects. (b) Illustration of the effect of crustal anisotropy on SKS splitting. The model consists of two anisotropic layers, one from a depth of 150-300 km with uniform 5% anisotropy corresponding to a 1.5 s split time and fast direction N80°E and one from 20-35 km with properties corresponding to the model of Castellanos et al. (2019). This model has an average crustal anisotropy of 10%. Background color illustrates the change in split time due to the addition of this anisotropic crustal layer.

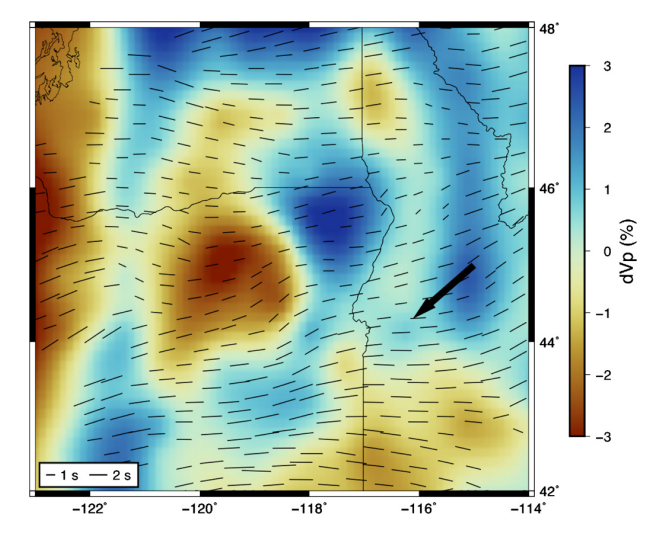


Fig. 10. SKS results from Fig. 5c plotted over P-wave velocity structure at 195 km depth from the tomographic image of Stanciu and Humphreys (2020). Arrow shows direction of absolute plate motion (from NNR-MORVEL56, Argus et al., 2011). We observe a good correspondence between regional variations in the fast splitting direction and the geometry of seismic anomalies, and the region of NE Oregon where splitting behavior is complex coincides with the largest velocity anomalies.

served fast polarization direction. In eastern Oregon, we observe significant differences in anisotropy over distances comparable to the size of the sensitivity kernel. This leads us to think that lateral heterogeneity in anisotropy is the most likely explanation for complex splitting results.

To investigate the effects of crustal anisotropy, we use a model with two anisotropic layers: a 'mantle' layer from a depth of 200-300 km with 5% anisotropy oriented N80°E (equivalent to a split time of 1.5 s) and a crustal layer from 20-35 km with properties according to the results of Castellanos et al. (2019). The forward model predicts that the crustal layer produces approximately 0.5 s of variation in the splitting time, but has no noticeable ef-

fect on the fast directions (Fig. 9a). Furthermore, the effect of the crustal layer is to reduce splitting time in the south (where crustal anisotropy is approximately orthogonal to the observed splitting direction) and increase it in NE Oregon. Castellanos et al. (2019) also find minimal crustal anisotropy in northeast Oregon, where our observed splitting is smallest in magnitude and most complex. Although the variation in split time inferred for crustal anisotropy is comparable to observed variations, this discrepancy suggests that crustal anisotropy is not the cause of complex behavior.

4. Discussion

We considered a set of reasons for the different splitting behavior in northeast Oregon: crustal anisotropy, vertically varying mantle anisotropy, lateral mantle anisotropic heterogeneity. Crustal anisotropy may produce significant changes in observed splitting times, but does not appear to affect the fast axis orientation, and the changes in splitting times due to imaged crustal anisotropy are inconsistent with observations. Mantle anisotropy in NE Oregon likely varies with depth, but the inconsistent performance of the two layer model suggests that vertically varying anisotropy is not the only cause. We hypothesize that the splitting behavior is a result of upper mantle anisotropy that varies both vertically and laterally, but one that maintains an observable degree of coherency at length scales of 100 km and more.

The upper mantle in the Pacific Northwest is strongly heterogeneous on the scale of $\sim 50~\rm km$ seismic wavelengths (Fig. 10 Schmandt and Lin, 2014; Stanciu and Humphreys, 2020; Gao and Shen, 2014). Prominent seismically imaged structures in the Pacific Northwest are the high-velocity Juan de Fuca slab, low-velocity anomalies under north central Oregon and the Snake River Plain, and two separate high-velocity bodies beneath northeast Oregon and central Idaho. Darold and Humphreys (2013) argue that the latter structures are fragments of Farallon oceanic lithosphere that delaminated from the North American continent at approximately 16 and 53 Ma, respectively. Mantle flow associated with their sinking following delamination would have occurred from 16-55 Ma; however, other factors such as absolute plate motion, Cascadia sub-

duction and slab rollback (e.g., Druken et al., 2011) and plume flattening (e.g., Lowry et al., 2000) are also likely to be important to the overall pattern of mantle flow. Any anisotropy produced by asthenospheric flow during their delamination would likely have been overprinted by the last 16 million years of strain since we expect 16 million years of accumulated strain to exceed that required to reset anisotropy (i.e., strain of 1-2, Skemer et al., 2012).

The observed complex Pacific Northwest seismic tomography (Fig. 10 suggests several reasons for the imaged heterogeneity (see also Lin et al., 2011). The relatively high-velocity mantle below 100 km is cooler, more viscous and presumably is subducted ocean lithosphere (Stanciu and Humphreys, 2020; Darold and Humphreys, 2013). The slab anisotropy may not align with present flow-induced anisotropy elsewhere in the upper mantle (Audet, 2013). For this lithosphere we may expect 'fossil' anisotropy aligned with the spreading direction at the site of lithosphere formation, perhaps modified by slab bending.

In contrast to anisotropy in the relatively high-velocity mantle, asthenospheric anisotropy is thought to indicate young mantle flow. Geodynamic modeling studies (e.g., Becker et al., 2006; Liu and Stegman, 2011; Wang and Becker, 2019; Zhou et al., 2018) have had success matching splitting-derived anisotropy in the western U.S. with coupled models of mantle flow and fabric development. In general, geodynamic models agree that ENE-WSW oriented anisotropy in the PNW is due to ENE-directed mantle flow relative to the North American plate. In addition, near the actively subducting Juan de Fuca slab (the north-trending fast structure near longitude —121), slab descent would tend to align anisotropy with top-side and bottom-side corner flow.

However, geodynamic models do not perform well at matching smaller-scale variations in asthenospheric anisotropy. Wang and Becker (2019) find that including strong cratonic roots and continental-scale mantle density structure inferred from seismic images significantly improves predicted anisotropy over models of plate-driven flow alone, but including higher-resolution models of density and craton geometry does not improve the fit to observations. Because the regional models perform well, we believe the assumption that anisotropy indicates horizontal mantle flow is valid, but it may not hold well on small scales.

The perpendicularity of anisotropy near the Juan de Fuca slab is expected for flow near a sinking body. In contrast, the frequent tendency for back arc anisotropy to parallel the mantle seismic structures suggests that flow there is more a consequence of flow deflection by the seismically fast structures than it is by any negative buoyancy of these structures. This may explain the observation of Wang and Becker (2019) that small-scale anomalies of presumed negative buoyancy do not improve their modeled fit to the anisotropy field. It appears to us that the two different relationships between mantle anisotropy and seismic velocity define two mantle flow domains.

Geodetic observations indicate that crustal deformation in the Pacific Northwest occurs primarily as rigid block rotation around a pole in central Idaho (McCaffrey et al., 2013), accommodated at its northern margin by shortening along the Yakima fold and thrust belt. The discrepancy between crustal and mantle deformation implies that the basal tractions resulting from mantle flow are not strong enough to deform the crust (McCaffrey et al., 2013). In support of this conclusion, Lin et al. (2011) and Castellanos et al. (2019, 2020) find that crustal anisotropy in the region (and inferred lower crustal flow) does not correlate with geodetically predicted mantle strain nor with the mantle anisotropy, and propose that at the scale of the Pacific Northwest, horizontal basal tractions applied by horizontal mantle flow are decoupled from the crustal deformation.

5. Conclusions

We use a largely automated method to compile approximately 3100 non-null shear-wave splitting measurements in the northwest United States. Our measurements are generally consistent with previous studies using different methodologies, but our study has much improved resolution.

Shear-wave splitting in the northwest United States appears to be roughly consistent with a simple model of anisotropy, with fast directions trending west-southwest. We attribute this to simple shear flow driven by motion of the North American plate, with the systematic deviations attributable to flow modification by the Cascadia subduction zone, and to $\sim\!200\text{-km}$ scale-length upper mantle structure. We observe particularly large split times, and characteristics of simple anisotropy, in the High Lava Plains and Snake River Plain regions (Fig. 1). Observed fast directions suggest west oriented flow beneath SE Oregon.

The shear-wave splitting signal in NE Oregon expresses an anisotropy that is inconsistent with layered models. We argue that this is a result of an anisotropic upper mantle structure that varies strongly both vertically and laterally, associated with the numerous pieces of abandoned oceanic lithosphere imaged under the Pacific Northwest.

6. Acknowledgments

The facilities of IRIS Data Services, and specifically the IRIS Data Management Center, were used for access to waveforms, related metadata, and/or derived products used in this study. IRIS Data Services are funded through the Seismological Facilities for the Advancement of Geoscience (SAGE) Award of the National Science Foundation under Cooperative Support Agreement EAR-1851048. Plots were made using GMT software (Wessel and Smith, 1998). We also acknowledge many useful discussions with Jorge Castellanos and Rob Clayton, and we appreciate the constructive advice of two anonymous reviewers. Funding was provided by NSF grants EAR-1547594 and EAR-1727451.

Declaration of competing interest

The authors declare that they have no known competing financial interests or personal relationships that could have appeared to influence the work reported in this paper.

References

Argus, D.F., Gordon, R.G., DeMets, C., 2011. Geologically current motion of 56 plates relative to the no-net-rotation reference frame. Geochem. Geophys. Geosyst. 12. https://doi.org/10.1029/2011GC003751.

Audet, P., 2013. Seismic anisotropy of subducting oceanic uppermost mantle from fossil spreading. Geophys. Res. Lett. 40, 173–177.

Becker, T.W., Schulte-Pelkum, V., Blackman, D.K., Kellogg, J.B., O'Connell, R.J., 2006. Mantle flow under the western United States from shear-wave splitting. Earth Planet. Sci. Lett. 237 (3-4), 235-251.

Bowman, J.R., Ando, M., 1987. Shear-wave splitting in the upper-mantle wedge above the Tonga subduction zone. Geophys. J. Int. 88 (1), 25–41.

Castellanos, J.C., Perry-Houts, J., Clayton, R.W., Humphreys, E., 2019. Crustal anisotropy as a window to mantle dynamics: a case study on the western United States. In: 2019 AGU Fall Meeting. San Francisco. Abstract presented.

Castellanos, J.C., Perry-Houts, J., Clayton, R.W., Kim, Y., Stanciu, A.C., Niday, B., Humphreys, E., 2020. Seismic anisotropy reveals crustal flow driven by mantle vertical loading in the Pacific NW. Under revision at Science Advances.

Chevrot, S., 2000. Multichannel analysis of shear-wave splitting. J. Geophys. Res., Solid Earth 105 (B9), 21579–21590.

Crotwell, H.P., Owens, T.J., Ritsema, J., 1999. The TauP Toolkit: flexible seismic traveltime and ray-path utilities. Seismol. Res. Lett. 70 (2), 154–160.

Darold, A., Humphreys, E., 2013. Upper mantle seismic structure beneath the Pacific Northwest: a plume-triggered delamination origin for the Columbia river flood basalt eruptions. Earth Planet. Sci. Lett. 365, 232–242.

Druken, K.A., Long, M.D., Kincaid, C., 2011. Patterns in seismic anisotropy driven by rollback subduction beneath the High Lava Plains. Geophys. Res. Lett. 38 (13).

- Favier, N., Chevrot, S., 2003. Sensitivity kernels for shear wave splitting in transverse isotropic media. Geophys. J. Int. 153 (1), 213–228.
- Gao, H., Shen, Y., 2014. Upper mantle structure of the Cascades from full-wave ambient noise tomography: evidence for 3D mantle upwelling in the back-arc. Earth Planet. Sci. Lett. 390, 222–233.
- Karato, S.-i., Jung, H., Katayama, I., Skemer, P., 2008. Geodynamic significance of seismic anisotropy of the upper mantle: new insights from laboratory studies. Annu. Rev. Earth Planet. Sci. Lett. 36, 59–95. https://doi.org/10.1146/annurev.earth.36. 031207.124120.
- Lin, F.-C., Ritzwoller, M.H., Yang, Y., Moschetti, M.P., Fouch, M.J., 2011. Complex and variable crustal and uppermost mantle seismic anisotropy in the western United States. Nat. Geosci. 4 (1), 55.
- Liu, L., Stegman, D.R., 2011. Segmentation of the Farallon slab. Earth Planet. Sci. Lett. 311 (1–2), 1–10.
- Long, M.D., Gao, H., Klaus, A., Wagner, L.S., Fouch, M.J., James, D.E., Humphreys, E., 2009. Shear wave splitting and the pattern of mantle flow beneath eastern Oregon. Earth Planet. Sci. Lett. 288 (3–4), 359–369.
- Long, M.D., Silver, P.G., 2009. Shear wave splitting and mantle anisotropy: measurements, interpretations, and new directions. Surv. Geophys. 30, 407–461. https://doi.org/10.1007/s10712-009-9075-1.
- Lowry, A.R., Ribe, N.M., Smith, R.B., 2000. Dynamic elevation of the Cordillera, western United States. J. Geophys. Res., Solid Earth 105 (B10), 23371–23390.
- McCaffrey, R., King, R.W., Payne, S.J., Lancaster, M., 2013. Active tectonics of northwestern U.S. inferred from GPS-derived surface velocities. J. Geophys. Res., Solid Earth 118 (2), 709–723.
- Menke, W., Levin, V., 2003. The cross-convolution method for interpreting SKS splitting observations, with application to one and two-layer anisotropic Earth models. Geophys. J. Int. 154 (2), 379–392.
- Romanowicz, B., Yuan, H., 2012. On the interpretation of SKS splitting measurements in the presence of several layers of anisotropy. Geophys. J. Int. 188 (3), 1129–1140
- Saltzer, R.L., Gaherty, J.B., Jordan, T.H., 2000. How are vertical shear-wave splitting measurements affected by variations in the orientation of azimuthal anisotropy with depth? Geophys. J. Int. 141 (2), 374–390.

- Schmandt, B., Lin, F.-C., 2014. P and S wave tomography of the mantle beneath the United States. Geophys. Res. Lett. 41 (18), 6342–6349.
- Silver, P.G., Chan, W.W., 1991. Shear wave splitting and subcontinental mantle deformation. J. Geophys. Res., Solid Earth 96 (B10), 16429–16454.
- Silver, P.G., Savage, M.K., 1994. The interpretation of shear-wave pslitting parameters in the presence of two anisotropic layers. Geophys. J. Int. 119 (3), 949–963.
- Skemer, P., Warren, J.M., Hirth, G., 2012. The influence of deformation history on the interpretation of seismic anisotropy. Geochem. Geophys. Geosyst. 13, Q03006. https://doi.org/10.1029/2011GC003988.
- Stanciu, C., Humphreys, E., 2020. Upper mantle tomography beneath the Pacific Northwest interior. Earth Planet. Sci. Lett. 539. https://doi.org/10.1016/j.epsl. 2020.116214. In press.
- Wagner, L.S., Long, M.D., 2013. Distinctive upper mantle anisotropy beneath the High Lava plains and Eastern Snake river plain, Pacific Northwest, USA. Geochem. Geophys. Geosyst. 14 (10), 4647–4666.
- Wang, W., Becker, T.W., 2019. Upper mantle seismic anisotropy as a constraint for mantle flow and continental dynamics of the North American plate. Earth Planet. Sci. Lett. 514, 143–155.
- Wessel, P., Smith, W.H., 1998. New, improved version of generic mapping tools released. Eos Trans. AGU 79 (47), 579.
- Wüstefeld, A., Bokelmann, G., Zaroli, C., Barruol, G., 2008. SplitLab: a shear-wave splitting environment in Matlab. Comput. Geosci. 34 (5), 515–528.
- Yang, B.B., Liu, K.H., Dahm, H.H., Gao, S.S., 2016. A uniform database of teleseismic shear-wave splitting measurements for the western and central United States: December 2014 update. Seismol. Res. Lett. 87 (2A), 295–300.
- Zhou, Q., Hu, J., Liu, L., Chaparro, T., Stegman, D.R., Faccenda, M., 2018. Western US seismic anisotropy revealing complex mantle dynamics. Earth Planet. Sci. Lett. 500, 156–167.